Lyapunov Exponents of a Simple Stochastic Model of the Thermally and Wind-Driven Ocean Circulation

Adam Hugh Monahan *

Institut für Mathematik, Humboldt-Universität zu Berlin

Unter den Linden 6, 10099 Berlin, Germany

(email: monahana@uvic.ca)

Revised draft, submitted to Dynamics of Atmospheres and Oceans

August 8, 2002

*Present Address: School of Earth and Ocean Sciences, University of Victoria, P.O. Box 3055 STN CSC,Victoria BC, Canada, V8P 5C2

Abstract

A reformulation of the simple model of the thermally and wind-driven ocean circulation introduced by Maas (1994) is considered. Under a realistic range of forcing parameters, this model displays multiple attractors, corresponding to thermally direct and indirect circulations. The fixed point associated with the thermally direct circulation is unstable for a broad range of parameters, leading to limit cycles and chaotic behaviour. It is demonstrated that if weather variability is parameterised as stochastic perturbations to the mechanical and buoyancy fluxes, then the leading Lyapunov exponent of the circulation can become positive for sufficiently strong fluctuations in parameter ranges where it is deterministically zero. If the fluctuations are sufficiently small that the stochastic trajectories are not too far from the deterministic attractor, it is demonstrated that the sign of the leading Lyapunov exponent can have a substantial effect on the predictability of the system.

1 Introduction

The climate system displays variability on spatial and temporal scales over many orders of magnitude, such that this variability is generally coupled across scales. In any tractable model of the climate system, there will be a broad range of spatial and temporal scales that cannot be represented explicitly, but have a nontrivial aggregate effect on the dynamics of the resolved scales. The representation of the net effect of unresolved processes on the resolved variables is the problem of subgrid-scale parameterisation. The separation between resolved and unresolved scales of variability is not unique, and depends on the class of models under consideration. In this study, the terms "weather" and "climate" will be used for variables representing processes on the unresolved and on the resolved scales, respectively.

The traditional approach to the parameterisation problem is to model the aggregate effect of the weather variables on the dynamics of the climate variables as a deterministic function of the climate state, assuming that each configuration of the resolved variables is associated with a unique net effect from the unresolved scales. A degenerate deterministic parameterisation, in which certain processes are ignored altogether, is also commonly used. A second approach, first suggested by Hasselmann (1976), represents the rapidly fluctuating and chaotic weather variables by stochastic processes. Although this parameterisation appears ad hoc, it can in fact be rigorously justified if the temporal autocorrelation function of the weather variable decays sufficiently rapidly, and if the timescale separation between weather and climate variables is sufficiently large (Penland, 2001). Although such infinite timescale separations do not occur in the climate system, the stochastic parameterisation of weather variability has demonstrated its utility in problems ranging from sea surface temperature spectra (e.g. Hasselmann, 1976) to El Niño/Southern Oscillation dynamics (e.g. Penland, 2000), to decadal-scale variability of the thermohaline circulation (e.g. Griffies and Tziperman, 1995).

A basic issue in climate dynamics is the predictability of future climate states. A quantitative measure of predictability is the leading Lyapunov exponent, λ, which is an intrinsic property of the climate dynamical system (Ott, 1993; Kloeden and Platen, 1992). If this

quantity is positive, the distance between two initially close climate states increases exponentially as a function of time until it is of the same size as the climate attractor; by this point, all predictability has been lost. If λ is negative, the trajectories starting from two initially close states asymptotically converge exponentially, although finite-time divergence is possible (Farrell and Ioannou, 1996a).

The presence of weather fluctuations can have two distinct effects on the predictability of the climate state. The first is straightforward: if weather fluctuations displace the trajectory of the climate state substantially away from the deterministic attractor, then its predictability will be limited by the inherent unpredictability of the weather state on climate timescales. The second effect is more subtle: the presence of fluctuations can lead to a positive λ in systems for which $\lambda < 0$ in the absence of weather noise. That is, the presence of weather noise can induce sensitivity to initial conditions in the climate state. If the strength of the fluctuations is sufficiently small that the random trajectories of the climate system do not stray too far from the deterministic attractor, then the sign of the leading Lyapunov exponent will have a determining effect upon predictability. This phenomenon, which can be described as "noise-induced chaos", has been demonstrated in Hamiltonian systems both numerically (e.g. Bulsara et al., 1990; Schimansky-Geier and Herzel, 1993) and analytically (Arnold et al., 2001). Farrell and Ioannou (1996b, 1999) demonstrated that noise can change the sign of the leading Lyapunov exponents of linear nonautonomous systems derived from β-channel models of midlatitude atmospheric variability. Moore (1999) considered the effects of weather noise on finite-time error growth in a fully nonlinear barotropic two-gyre ocean model, but because of computational limitations was not able to evaluate the Lyapunov exponents.

In this study, we will consider the effects of weather fluctuations in both the mechanical and buoyancy forcing on the leading Lyapunov exponent of a fully nonlinear, albeit highly simplified, model of the thermally and wind-driven ocean circulation developed by Maas (1994). It will be shown that the presence of stochastic fluctuations can lead to an increase or a decrease in the leading Lyapunov exponent, relative to the deterministic value. In particular, it will be shown that there are regions of parameter space in which very small

stochastic perturbations can change the sign of the leading Lyapunov exponent from negative to positive, inducing sensitivity to initial conditions in the climate variables.

The original study of Maas (1994) considered the effects of rotation on the existence of multiple circulation states; consequently, the Coriolis parameter was used as the bifurcation parameter. In this study, the rotation rate is fixed, and the bifurcation structure as a function of mechanical dissipation will be studied. Therefore, a somewhat different formulation of Maas' model is required. This reformulation is presented in Section 2. The stochastic generalisation of this model and the associated mathematical formalism are considered in Section 3. Section 4 presents an analysis of the deterministic system over the parameter ranges considered. The main results of the paper, describing the noise-induced sensitivity to initial conditions in the model and the resulting changes to predictability, are presented in Section 5. Section 6 contains a discussion and conclusions.

2 The Maas Model of the Thermally and Wind-Driven Ocean Circulation

The system of equations derived by Maas (1994) describe the coupled dynamics of oceanic angular momentum and isopycnal surfaces in a rectangular ocean basin on an f-plane, driven by thermal and mechanical forcing from the atmosphere. The basin is of length L in the zonal and meridional directions and of depth H; the volume of the basin is denoted $V = HL^2$. A coordinate system is employed such that the origin is at the geometrical centre of the box. Rescaled density and pressure are defined by:

$$\rho = \frac{\rho_* - \rho_0}{\delta\rho} \tag{1}$$

$$p = \frac{p_* - p_0}{\rho_0}, \tag{2}$$

where ρ_* is the original, dimensional density, ρ_0 is a constant reference density, $\delta\rho$ is a density fluctuation scale (to be specified later), p_* is the dimensional pressure, and p_0 is a reference pressure hydrostatically related to ρ_0. A fundamental approximation, which is necessary to

close the model, is that isopycnal surfaces are planar and parallel:

$$\rho = x\overline{\rho}_x + y\overline{\rho}_y + z\overline{\rho}_z, \tag{3}$$

where

$$\overline{\rho}_x = \frac{\int dV x\rho}{\int dV x^2} \tag{4}$$

and similarly for $\overline{\rho}_y$ and $\overline{\rho}_z$. The dynamics of the basin-averaged angular momentum

$$\mathbf{L} = \frac{1}{V}\int dV \mathbf{x} \times \mathbf{u}, \tag{5}$$

where $\mathbf{x}$ and $\mathbf{u}$ are respectively the coordinate and velocity fields, can be shown to be given by

$$\frac{d}{dt}\mathbf{L} + \frac{f}{2}\mathbf{k} \times \mathbf{L} = -\frac{g'H^2}{12}(-\overline{\rho}_y\mathbf{i} + \overline{\rho}_x\mathbf{j}) - R\mathbf{L} + \mathbf{T}, \tag{6}$$

where $\mathbf{i}, \mathbf{j}$, and $\mathbf{k}$ are respectively unit vectors in the x, y, and z directions, $g' = g\delta\rho/\rho_0$ is the reduced gravity, and $\mathbf{T}$ denotes the surface angular momentum flux from wind forcing:

$$\mathbf{T} = \frac{1}{V}\int\int dxdy \left(-\frac{H}{2}\tau^{(y)}\mathbf{i} + \frac{H}{2}\tau^{(x)}\mathbf{j} + (x\tau^{(y)} - y\tau^{(x)})\mathbf{k}\right). \tag{7}$$

(Maas, 1994). The following assumptions have been used in the derivation of equation (6):

- The Boussinesq approximation
- The frictional effects of boundary layers along the rigid walls can be represented by a diagonal Rayleigh friction tensor:

$$R = \begin{pmatrix} r_h & 0 & 0 \\ 0 & r_h & 0 \\ 0 & 0 & r_v \end{pmatrix}, \tag{8}$$

  and
- The nonhydrostatic component of the pressure torque is negligible.

The equation of motion for the density gradient vector $\nabla\overline{\rho} = \overline{\rho}_x\mathbf{i} + \overline{\rho}_y\mathbf{j} + \overline{\rho}_z\mathbf{k}$ is:

$$D\frac{d}{dt}\nabla\overline{\rho} + \frac{1}{2}\nabla\overline{\rho} \times \mathbf{L} = -K\nabla\overline{\rho} + \mathbf{F}, \tag{9}$$

where

$$D = \begin{pmatrix} \frac{L^2}{12} & 0 & 0 \\ 0 & \frac{L^2}{12} & 0 \\ 0 & 0 & \frac{H^2}{12} \end{pmatrix} \tag{10}$$

is a diagonal matrix of geometrical factors and

$$K = \begin{pmatrix} K_h & 0 & 0 \\ 0 & K_h & 0 \\ 0 & 0 & K_v \end{pmatrix} \tag{11}$$

is the diffusivity tensor. The vector

$$\mathbf{F} = \frac{1}{V} \int \int dxdy \left(x\mathbf{i} + y\mathbf{j} + \frac{H}{2}\mathbf{k} \right) Q \tag{12}$$

denotes the moments of the surface buoyancy flux, Q. With specified moments of the external mechanical and buoyancy forcing, $\mathbf{T}$ and $\mathbf{F}$, equations (6) and (9) are a closed set of equations for the coupled dynamics of the basin-averaged angular momentum and isopycnal surfaces.

The following assumptions are made about the forcing functions $\tau^{(x,y)}$ and Q:

$$\tau^{(y)} = 0 \tag{13}$$

$$\tau^{(x)} = u_*^2 \sin\left(\frac{\pi y}{L}\right) \tag{14}$$

$$\int dxdy\, Q = 0 \tag{15}$$

$$Q = Q(y). \tag{16}$$

Assumption (15) implies that there is no net buoyancy flux into the ocean. With these assumptions, we obtain the simplified expressions

$$\mathbf{T} = -\frac{2L}{\pi^2 H} u_*^2 \mathbf{k} \tag{17}$$

$$\mathbf{F} = \frac{1}{LH} \int_{-L/2}^{L/2} dy\, yQ\mathbf{j}. \tag{18}$$

Equations (6) and (9) are nondimensionalised by rescaling the spatial variables by the corresponding ocean basin lengths and the time variable by a characteristic horizontal diffusion timescale:

$$[x, y, z, t] = \left(L, L, H, \frac{L^2}{12K_h} \right). \tag{19}$$

Defining $\delta\rho_e$ such that

$$[Q] = \frac{\delta\rho_e H K_h}{\delta\rho L^2} \tag{20}$$

and defining the scale of density fluctuations as

$$\delta\rho = \frac{12 K_h f \rho_0}{gH}, \tag{21}$$

we obtain the equations

$$\gamma\frac{d}{dt}\mathbf{L} + \frac{1}{2}\mathbf{k}\times\mathbf{L} = -\overline{\rho}_y\mathbf{i} + \overline{\rho}_x\mathbf{j} - \epsilon(L_1\mathbf{i} + L_2\mathbf{j} + rL_3\mathbf{k}) - \hat{T}\mathbf{k} \tag{22}$$

$$\frac{d}{dt}\nabla\overline{\rho} + \frac{1}{2}\nabla\overline{\rho}\times\mathbf{L} = -(\overline{\rho}_x\mathbf{i} + \overline{\rho}_y\mathbf{j} + \mu\overline{\rho}_z\mathbf{k}) + B_2\mathbf{j}, \tag{23}$$

where

$$\gamma = \frac{12K_h}{fL^2} \tag{24}$$

$$\epsilon = \frac{r_h}{f} \tag{25}$$

$$r = \frac{r_v}{r_h} \tag{26}$$

$$\hat{T} = \frac{2u_*^2 L}{\pi^2 f K_h H} \tag{27}$$

$$\mu = \frac{K_v L^2}{K_h H^2} \tag{28}$$

$$B_2 = \frac{\delta\rho_e}{\delta\rho}. \tag{29}$$

Equations (22) and (23) differ from equations (11a) and (11b) of Maas (1994). The original study by Maas was interested in the effect of rotation on the existence of multiple equilibria of circulation, and the equations of motion were nondimensionalised through dividing by the dissipation timescale r_h. This study is concerned with the effect of varying the dissipation strength at fixed rotation rate, so nondimensionalisation of the equations of motion has been accomplished by dividing through by f.

Adopting similar parameter values to those used in Maas (1994): $L = 5\times10^6$ m, $H = 5\times10^3$ m, $g = 10\text{ms}^{-2}$, $f = 10^{-4}\text{s}^{-1}$, $K_h = 10^2$ m^{2}s^{-1}, $K_v = 10^{-4}$ m^{2}s^{-1}, $u_* = 10^{-2}\text{ms}^{-1}$, $r_h = r_v = 10^{-7}\text{s}^{-1}$, $\delta\rho_e/\delta\rho = 1\times10^{-3}$, we obtain typical parameter values: $\gamma = 5\times10^{-7}$, $\epsilon = 10^{-3}$, $r = 1$, $\mu = 1$, $B_2 = 375$, and $\hat{T} = 2$. The nondimensional timescale is $L^2/12K_h = 660$ years.

The parameter γ, the ratio between the rotation and the horizontal diffusion timescales, is very small. To simplify equations (22), (23), the inertia of the angular momentum is ignored through the approximation $\gamma = 0$. This allows an explicit solution for the components of the density gradient in terms of the components of the angular momentum:

$$L_1 = \frac{1/2\overline{\rho}_x - \epsilon\overline{\rho}_y}{\epsilon^2 + 1/4} \tag{30}$$

$$L_2 = \frac{1/2\overline{\rho}_y + \epsilon\overline{\rho}_x}{\epsilon^2 + 1/4} \tag{31}$$

$$L_3 = -\frac{\hat{T}}{r\epsilon}. \tag{32}$$

Substituting (30) and (31) into (23), and rescaling $\nabla\overline{\rho}$ and B_2 by $(2\epsilon^2 + 1/2)^{-1}$, we obtain the following system of equations for the components of $\nabla\overline{\rho}$ only:

$$\frac{d}{dt}\overline{\rho}_x = -(1 - \epsilon\overline{\rho}_z)\overline{\rho}_x - \frac{1}{2}(L_3 - \overline{\rho}_z)\overline{\rho}_y \tag{33}$$

$$\frac{d}{dt}\overline{\rho}_y = \frac{1}{2}(L_3 - \overline{\rho}_z)\overline{\rho}_x - (1 - \epsilon\overline{\rho}_z)\overline{\rho}_y + B_2 \tag{34}$$

$$\frac{d}{dt}\overline{\rho}_z = -\mu\overline{\rho}_z - \epsilon(\overline{\rho}_x^2 + \overline{\rho}_y^2). \tag{35}$$

The equations for the horizontal components of $\nabla\overline{\rho}$ have the form of a damped, driven oscillator whose oscillation frequency and damping depend on $\overline{\rho}_z$. The dynamics of $\overline{\rho}_z$ resembles that of a driven overdamped spring.

At this point, we will note some of the physical constraints placed on the model by the various approximations that have gone into its derivation. First, meridional structure in the planetary vorticity is neglected: this model describes dynamics only on an f-plane. This has the effect of excluding Rossby waves from the "internal dynamics" of the model ocean. Second and third are the approximations that isopycnal surfaces are parallel planes and the neglect of non-hydrostatic pressure torques. These approximations ensure that isopycnal and isobaric surfaces coincide, and thus the geostrophic flow away from boundaries is barotropic. Consequently, much of the flow must be concentrated in narrow boundary layers near the walls. Relaxing these first three approximations greatly increases the dimensionality of the model (van der Schrier, 2000). Fourth, no coupling between the ocean and atmosphere is allowed in the model; the atmosphere appears only through surface boundary conditions

that are independent of the state of the ocean. The extent to which there exists a two-way coupling between the atmosphere and the ocean in middle latitudes remains a subject of debate (e.g. Timmermann et al., 1998 and Delworth and Greatbatch, 2000). Fifth, the model considers only a single component fluid: the individual contributions of salinity and temperature to the density field are not considered. This constraint has been addressed in a generalisation of the model presented in van der Schrier and Maas (1998); the original Maas (1994) model is considered in this study to keep the system of equations, and the space of parameters, as simple as possible. Despite the potential limitations outlined above, the model remains attractive because it follows from the full equations of motion via an explicit set of approximations. This is to be contrasted with, e.g., box models of the ocean circulation. While box are instructive, their derivation is generally heuristic. We will then approach the Maas model as an "ocean-like" system, conscious of the constraints described above.

3 Fluctuating External Forcing

So far, the mechanical forcing $\hat{T}$ (equivalently, L_3) and the buoyancy forcing B_2 have been treated as fixed constants. A parameterisation of weather fluctuations in the mechanical and thermal forcing is introduced through the addition of stochastic components to L_3 and B_2:

$$L_3 \rightarrow L_3 + \sigma_1 \dot{W}_1(t) \tag{36}$$

$$B_2 \rightarrow B_2 + \sigma_2 \dot{W}_2(t). \tag{37}$$

where $\dot{W}_j(t)$ $(j = 1, 2)$ are Gaussian white noise process:

$$< \dot{W}_j(t) > = 0 \tag{38}$$

$$< \dot{W}_i(t)\dot{W}_j(t') > = \delta(t - t')\delta_{ij}. \tag{39}$$

The angle brackets $< \cdot >$ denote the expectation operator. For simplicity, we have assumed that the fluctuations in buoyancy forcing and mechanical forcing are independent. Of course, because the surface winds play a central role in both momentum and buoyancy fluxes, there

is presumably some covariability between these fluctuations. However, as buoyancy fluxes are affected by a broad range of physical processes not directly connected to surface winds (e.g. cloudiness, precipitation rates), we will make the approximation that the two processes can be treated as independent.

With the introduction of white noise fluctuations in L_3 and B_2, equations (33)-(35) become a stochastic differential equation (SDE) in $\Re^3$, which is expressed in differential form as

$$d\overline{\rho}_x = \left[-(1-\epsilon\overline{\rho}_z)\overline{\rho}_x - \frac{1}{2}(L_3-\overline{\rho}_z)\overline{\rho}_y\right]dt - \frac{1}{2}\sigma_1\overline{\rho}_y \circ dW_1(t) \tag{40}$$

$$d\overline{\rho}_y = \left[\frac{1}{2}(L_3-\overline{\rho}_z)\overline{\rho}_x - (1-\epsilon\overline{\rho}_z)\overline{\rho}_y + B_2\right]dt + \frac{1}{2}\sigma_1\overline{\rho}_x \circ dW_1(t) + \sigma_2 dW_2 \tag{41}$$

$$d\overline{\rho}_z = \left[-\mu\overline{\rho}_z - \epsilon(\overline{\rho}_x^2+\overline{\rho}_y^2)\right]dt. \tag{42}$$

An introduction to the theory of SDEs is presented in Gardiner (1997). A noise term in an SDE is said to be additive if it does not depend on the state vector; otherwise, it is said to be multiplicative. Fluctuations in buoyancy forcing enter the SDE as additive noise, while fluctuations in mechanical forcing enter multiplicatively. While the interpretation of stochastic differentials associated with additive noise is unambiguous, care is required with the interpretation of multiplicative fluctuations. The open circle $\circ$ indicates that the stochastic differentials associated with fluctuating mechanical forcing are interpreted in the Stratonovich sense. Physically, this reflects the fact that the fluctuations in L_3 have a finite, although very short, autocorrelation time, and the white noise representation is an idealisation. Mathematically, Stratonovich differentials are attractive because the associated chain rule is that of classical calculus. Another form of the stochastic differential, due to Ito, yields SDEs that are more appropriate for numerical discretisation. A simple transformation rule connects the two interpretations; a process $\mathbf{Y}_t$ in $\Re^d$ solving the Stratonovich SDE:

$$d\mathbf{Y}_t = \mathbf{a}(t,\mathbf{Y}_t)dt + b(t,\mathbf{Y}_t)\circ d\mathbf{W}(t) \tag{43}$$

is also a solution of the Ito SDE

$$d\mathbf{Y}_t = \mathbf{a}^{(I)}(t,\mathbf{Y}_t)dt + b(t,\mathbf{Y}_t)d\mathbf{W}(t), \tag{44}$$

where

$$a_i^{(I)} = a_i + \frac{1}{2}\sum_{j,k} b_{kj}\partial_k b_{ij}. \tag{45}$$

and $\mathbf{W}(t)$ is an $\Re^p$ vector Wiener process with independent components. The $\Re^d$ vector functions $\mathbf{a}$ and $\mathbf{a}^{(I)}$ are referred to respectively as the Stratonovich and Ito drifts, and the $d \times p$ matrix function b is known as the diffusion. From (45), it is clear that in the special case that b does not depend on the state variable $\mathbf{Y}_t$ (additive noise), the Ito and Stratonovich SDEs coincide. We shall have need in the following discussion to work with both Ito and Stratonovich SDEs. A detailed discussion of the differences between Stratonovich and Ito SDEs is provided in Penland (2001) and in Gardiner (1997).

It is interesting to note that multiplicative stochasticity enters the density dynamics naturally via fluctuations in the strength of the gyre circulation. Random fluctuations in the gyre circulation were introduced heuristically in Monahan et al. (2001) and in Monahan (2001) to justify the presence of a multiplicative noise term in a simple box model of the thermohaline circulation; in the Maas model such terms follow naturally from the equations of motion.

Equations (40)-(42) are too complicated to admit an analytic solution for general parameter values. In consequence, we must take recourse to numerical approximations to analyse this system. The most straightforward numerical approximation of (40)-(42) is a forward-Euler discretisation (Kloeden and Platen, 1992). Discretising time with timestep δ, such that $t_k = k\delta$, the forward-Euler approximation to the Ito SDE yields the recursion relation:

$$\mathbf{Y}_{t_{k+1}} = \mathbf{Y}_{t_k} + \mathbf{a}^{(I)}(t_k, \mathbf{Y}_{t_k})\delta + b(t_k, \mathbf{Y}_{t_k})\sqrt{\delta}\xi_k, \tag{46}$$

where the ξ_k are independent, mean-zero, unit-variance, Gaussian random vectors in $\Re^p$ with independent components. The square root of the timestep appears in the stochastic term on the right-hand side of (46) because the *variance* of an increment of a Wiener process increases linearly with time:

$$< (W_{t_{k+1}} - W_{t_k})^2 >= \delta, \tag{47}$$

so the increment itself scales as the square root of the timestep.

To obtain the discretised form of equations (40)-(42), they must first be transformed into Ito form using the transformation rule (45). Here, b is the matrix:

$$\mathbf{b}(\nabla\overline{\rho}) = \begin{pmatrix} -\frac{1}{2}\sigma_1\overline{\rho}_y & 0 \\ \frac{1}{2}\sigma_1\overline{\rho}_x & \sigma_2 \\ 0 & 0 \end{pmatrix} \tag{48}$$

so

$$\frac{1}{2}\sum_{j,k} b_{kj}\partial_k b_{ij} = -\frac{\sigma_1^2}{8}(\overline{\rho}_x, \overline{\rho}_y, 0)_i. \tag{49}$$

The Ito form of equations (40)-(42) is

$$d\overline{\rho}_x = \left[-\left(1 - \epsilon\overline{\rho}_z + \frac{\sigma_1^2}{8}\right)\overline{\rho}_x - \frac{1}{2}(L_3 - \overline{\rho}_z)\overline{\rho}_y\right]dt - \frac{1}{2}\sigma_1\overline{\rho}_y dW_1(t) \tag{50}$$

$$d\overline{\rho}_y = \left[\frac{1}{2}(L_3 - \overline{\rho}_z)\overline{\rho}_x - \left(1 - \epsilon\overline{\rho}_z + \frac{\sigma_1^2}{8}\right)\overline{\rho}_y + B_2\right]dt + \frac{1}{2}\sigma_1\overline{\rho}_x dW_1(t) + \sigma_2 dW_2 \tag{51}$$

$$d\overline{\rho}_z = \left[-\mu\overline{\rho}_z - \epsilon(\overline{\rho}_x^2 + \overline{\rho}_y^2)\right]dt, \tag{52}$$

which is the form appropriate for discretisation and numerical approximation.

A quantity of central interest in the study of both deterministic and stochastic dynamical systems is the leading Lyapunov exponent, which determines the sensitivity of solutions to small perturbations in the initial conditions. If the leading Lyapunov exponent of an SDE is negative, trajectories with slightly different initial conditions but driven by the same noise realisation will asymptotically converge to the same random trajectory at an exponential rate (although the error may grow for a finite time; Farrell and Ioannou, 1996a). Conversely, if the leading Lyapunov exponent is positive, initial differences between two trajectories will amplify until the average difference is comparable to the size of the attractor. The theory of Lyapunov exponents for SDEs is reviewed in Appendix A; deterministic Lyapunov exponents are obtained in the limit that the strength of fluctuations vanishes. Briefly, for a given realisation $\nabla\overline{\rho}(t)$ of (40)-(42), the leading Lyapunov exponent of the system is given by

$$\lambda = \lim_{t\to\infty}\frac{1}{t}\int_0^t q(\mathbf{S}(u))du, \tag{53}$$

where

$$q(\mathbf{S}) = q^0(\mathbf{S}) + \frac{1}{2}\mathbf{S}^T[B(\nabla\overline{\rho}) + B(\nabla\overline{\rho})^T]B(\nabla\overline{\rho})\mathbf{S} - (q^1(\mathbf{S}))^2, \tag{54}$$

in which

$$q^0(\mathbf{S}(t)) = \mathbf{S}(t)^T A(\nabla\overline{\rho}(t))\mathbf{S}(t) \quad (55)$$

$$q^1(\mathbf{S}(t)) = \mathbf{S}(t)^T B(\nabla\overline{\rho}(t))\mathbf{S}(t). \quad (56)$$

In the above, A and B are the drift and diffusion operators obtained from (40)-(42) linearised around the trajectory $\nabla\overline{\rho}(t)$:

$$A(\nabla\overline{\rho}(t)) = \begin{pmatrix} -(1-\epsilon\overline{\rho}_z(t)) & -\frac{1}{2}(L_3-\overline{\rho}_z(t)) & \left(\frac{1}{2}\overline{\rho}_y(t)+\epsilon\overline{\rho}_x(t)\right) \\ \frac{1}{2}(L_3-\overline{\rho}_z(t)) & -(1-\epsilon\overline{\rho}_z(t)) & \left(-\frac{1}{2}\overline{\rho}_x(t)+\epsilon\overline{\rho}_y(t)\right) \\ -2\epsilon\overline{\rho}_x(t) & -2\epsilon\overline{\rho}_y(t) & -\mu \end{pmatrix} \quad (57)$$

$$B(\nabla\overline{\rho}(t)) = \begin{pmatrix} 0 & -\frac{1}{2}\sigma_1 & 0 \\ \frac{1}{2}\sigma_1 & 0 & 0 \\ 0 & 0 & 0 \end{pmatrix}. \quad (58)$$

As is described in Appendix A, the process $\mathbf{S}(t)$ is the projection onto the unit sphere in $\Re^d$ of the process satisfying the SDE (40)-(42) linearised around the realisation $\nabla\overline{\rho}(t)$; $\mathbf{S}(t)$ satisfies the SDE

$$d\mathbf{S} = (A(\nabla\overline{\rho}) - q^0(\mathbf{S})I)\mathbf{S}dt + (B(\nabla\overline{\rho}) - q^1(\mathbf{S})I)\mathbf{S} \circ dW_1, \quad (59)$$

in which the Wiener process $W_1(t)$ is the same as that used to generate the realisation $\nabla\overline{\rho}(t)$, and I is the identity matrix in $\Re^d$. Note that the equation for $\mathbf{S}(t)$ does not explicitly involve the additive noise process $W_1(t)$, which vanishes in the linearisation. This process is present implicitly in (59) through the realisation $\nabla\overline{\rho}(t)$ around which the dynamics are linearised. From the Multiplicative Ergodic Theorem of Oseledec (Arnold, 1998), the limit (53) is *unique* and *non-random*; that is, it is independent of the particular realisation of $\nabla\overline{\rho}(t)$. Note that because $B(\nabla\overline{\rho}(t))$ is an antisymmetric matrix, $q(\mathbf{S}(t)) = q^0(\mathbf{S}(t))$.

To estimate numerically the Lyapunov exponents of the system, the following procedure is followed:

1. The Stratonovich SDEs (40)-(42) are transformed into the equivalent Ito form (50)-(52)

2. These Ito equations are discretised using (46)

3. A time $T = N\delta$ is defined to replace ∞ in the limit (53):

$$\lambda = \frac{1}{T}\int_0^T q(\mathbf{S}(t))dt \tag{60}$$

4. A realisation of $\{\xi_k\}_{k=1}^N$ is generated

5. This realisation of ξ is used to integrate the discretised forms of the SDE for $\nabla\overline{\rho}(t)$

6. The realisation of ξ from Step 4 and the realisation of $\nabla\overline{\rho}$ from Step 5 are used to integrate the discretised version of the Ito form of (59)

7. The limit (53) is evaluated

The integration time T is taken to be sufficiently large that differences between values of λ obtained using different realisations of ξ are small.

In this study, we will consider the dynamics of the stochastic system (40)-(42) (equivalently, (50)-(52)) for a range of values of ϵ and σ_1, with fixed "realistic" values of $L_3 = -50$ and $B_2 = 500$. Note that holding L_3 constant as ϵ varies implies that $\hat{T}$ is taken to scale as ϵ.

4 Deterministic Analysis

Figure 1 displays plots of the stationary solutions $(\overline{\rho}_x^*, \overline{\rho}_y^*, \overline{\rho}_z^*)$ of the deterministic system (33)-(35) as functions of ϵ; Figure 2 displays the corresponding values of the angular momentum components L_1 and L_2. The fixed points $\nabla\overline{\rho}^*$ are given by the equations

$$\overline{\rho}_x^* = \frac{-\frac{1}{2}(L_3 - \overline{\rho}_z^*)B_2}{(1-\epsilon\overline{\rho}_z^*)^2 + \frac{1}{4}(L_3 - \overline{\rho}_z^*)^2} \tag{61}$$

$$\overline{\rho}_y^* = \frac{(1-\epsilon\overline{\rho}_z^*)B_2}{(1-\epsilon\overline{\rho}_z^*)^2 + \frac{1}{4}(L_3 - \overline{\rho}_z^*)^2}, \tag{62}$$

where $\overline{\rho}_z^*$ is a solution of the cubic equation

$$\left[(1-\epsilon\overline{\rho}_z^*)^2 + \frac{1}{4}(L_3 - \overline{\rho}_z^*)^2\right]\overline{\rho}_z^* = -\frac{\epsilon B_2^2}{\mu}. \tag{63}$$

Clearly, $\overline{\rho}_z^*$ is always negative: all fixed points correspond to a stable stratification. As well, $\overline{\rho}_y^*$ always takes the same sign as B_2. The fixed points of the system are characterised by three

branches, which meet in saddle-node bifurcations at $\log_{10}\epsilon \simeq -3.70$ and $\log_{10}\epsilon \simeq -1.73$. For ϵ between these values, the system displays three fixed points. The upper branch, which survives for very small values of ϵ, is characterised by small density gradients. It describes weakly stratified flow with a weak thermally indirect meridional circulation in which water rises at the poleward end of the basin and sinks at the equatorward end. On most of this branch, the basic density gradient tendency balances (23) can be simplified to:

$$\overline{\rho}^*_y L_3 \simeq -2\overline{\rho}^*_x \tag{64}$$

$$-\overline{\rho}^*_x L_3 \simeq 2B_2 \tag{65}$$

$$\overline{\rho}^*_x L_2 \simeq \overline{\rho}^*_y L_1. \tag{66}$$

From (65), we see that $\overline{\rho}^*_x$ is adjusted so that the tendency of $\overline{\rho}_y$ due to external buoyancy forcing is balanced by advection by the gyre circulation; as $B_2 > 0$ and $L_3 < 0$, $\overline{\rho}^*_x$ is positive. The y-gradient $\overline{\rho}^*_y$ adjusts to balance diffusion and gyre advection in the tendency equation (64) for $\overline{\rho}_x$. The overturning circulations described by L_1 and L_2, determined primarily by the balance between buoyancy torque and Coriolis torque (equations (30),(31)), are both positive and of magnitudes such that the associated advection terms in the $\overline{\rho}_z$ tendency equation are essentially in balance. The fixed points on this branch are always stable.

The middle branch describes a more strongly stratified ocean with a vigorous thermally-indirect circulation; fixed points on this branch are always unstable. The lower branch is characterised by strong density gradients and a thermally-direct overturning cell; the associated fixed points may be stable or unstable. On this branch, the interplay between forcing, advection, dissipation, and diffusion is more complicated than on the upper branch. This branch of solutions corresponds most closely to the present thermally-direct thermohaline circulation and will be the focus of the rest of this study.

The structure of the attractor around the thermally-direct branch for varying ϵ can be characterised by its intersection with the Poincaré section $\overline{\rho}_y = \overline{\rho}^*_y$. Figure 3 displays the values of $\overline{\rho}_x$ at which the trajectory crosses this surface, as a function of ϵ. The associated Poincaré map is defined as the map between the values of $\overline{\rho}_x$ at successive crossings of the Poincaré surface; the *period* of such a map is the number of iterations required for a point

to be mapped onto itself. The bifurcation structure on the thermally-direct branch displays the familiar period-doubling route to chaos for decreasing ϵ (Ott, 1993). For $\log_{10}\epsilon > -1.54$, the fixed point $\overline{\rho}_x^*$ is stable and the attractor is a fixed point with a period-1 Poincaré map. At $\log_{10}\epsilon \simeq -1.54$ there is a Hopf bifurcation; the attractor is a period-2 limit cycle whose amplitude grows as ϵ decreases. At $\log_{10}\epsilon \simeq -1.98$ the limit cycle bifurcates to a period-4 limit cycle, and at $\log_{10}\epsilon \simeq -2.25$ to a period-8 limit cycle. As ϵ is decreased still further, the attractor goes through a series of increasingly close period-doubling bifurcations until it is fully chaotic. From this point on, there are alternating windows in ϵ in which the attractor is a limit cycle or chaotic until there is a final reverse Hopf bifurcation to a stable fixed point, occurring just before the saddle-node bifurcation at $\log_{10}\epsilon \simeq -3.68$. Figure 4 displays the structure of the attractors at $\log_{10}\epsilon = -1.8, -2.2, -2.3, -2.4$, clearly illustrating the period-doubling transition to chaos. The locations of chaotic and non-chaotic attractors can be further quantified through consideration of the leading Lyapunov exponents of the system, displayed as a function of ϵ in the upper panel of Figure 3. These Lyapunov exponents were estimated using the procedure outlined in Section 3 (with $\sigma_1 = \sigma_2 = 0$). The variation of the Lyapunov exponents with ϵ reflects the bifurcation structure displayed in Figure 3. The leading Lyapunov exponents are negative where the attractor is a fixed point or a limit cycle, and positive where the attractor is chaotic. Figure 5 displays a blow-up of Figure 3 in the region of the transition to chaos.

The deterministic Maas model displays a rich structure over a "realistic" range of the mechanical friction parameter, ϵ. For certain parameter ranges, the thermally-direct attractors are fixed points or limit cycles with negative leading Lyapunov exponents and predictable trajectories. In other parameter ranges, the attractor around the branch of solutions corresponding to thermally-direct circulation is chaotic, with positive leading Lyapunov exponents, and trajectories are predictable for only a finite time. In the next section, the effect of stochastic weather fluctuations in the mechanical and buoyancy forcing on the sign of the Lyapunov exponents and the predictability of the system will be considered.

5 Lyapunov Exponents and Predictability of the Stochastic System

In the previous section, we considered the dynamics of the climate state described by the Maas model in the absence of weather variability; we now consider the effects of nonzero fluctuations in the mechanical and buoyancy forcing. Because the fluctuations in L_3 and B_2 are Gaussian, over very long times the system will make an arbitrarily large number of transitions between the thermally direct and indirect branches, and the stationary distribution will have mass in both regions. However, as is discussed in Monahan (2001), the stationary distribution is only relevant to the description of a system with multiple regimes if the average exit time of each regime is smaller than the longest physically-relevant timescale. For longer average exit times, the vast majority of realisations will remain within the basin of attraction in which they started, and it is the dynamics confined to this regime which are of physical relevance. In this study, we are concerned not with transitions between the thermally direct and indirect circulation branches, but with the effect of weather fluctuations on the dynamics along the thermally direct branch. In fact, the noise strengths considered in this study are sufficiently small that the average first exit time from the thermally-direct branch is substantially larger than the timescales under consideration. The definition of the leading Lyapunov exponent λ is based on the $t \to \infty$ limit of the average (53), and consequently involves dynamics around both the thermally direct and indirect branches. To characterise the local leading Lyapunov exponent on the thermally direct branch, the infinite limit is replaced by a large, but finite, time $\tilde{T}$. This time is large enough for the system to fully sample the local attractor, but much smaller than the average escape time of the thermally-direct regime. The infinite limit in (53) has already been replaced by a finite limit T for numerical reasons in Section 3; to evaluate numerically the leading Lyapunov exponent of the thermally-direct branch, we take the times T and $\tilde{T}$ to be the same. In the calculations presented here, we have taken $T = 2500$, with a timestep $\delta = 5 \times 10^{-4}$.

We first consider the effects of fluctuations in the mechanical forcing. Figure 6 displays sample trajectories on the thermally-direct branch for

$\log_{10}\epsilon = -1.8, -2.2, -2.3, -2.4$, perturbed by weak noise $\sigma_1 = 0.1, \sigma_2 = 0$. Because the fluctuations in mechanical forcing are weak, the stochastic trajectories lie close to the deterministic attractors displayed in Figure 4. For larger values of σ_1, individual stochastic trajectories display more substantial deviations from the deterministic trajectories, although they remain quite structured. This is illustrated in Figure 7 for the noise levels $\sigma_1 = 1, \sigma_2 = 0$.

Estimates of the leading Lyapunov exponents on the thermally-direct branch of the stochastic Maas model over a range of noise strengths σ_1 with $\sigma_2 = 0$ and $\log_{10}\epsilon = -2.0, -2.1, -2.2$ are displayed in Figure 8. For each pair of parameter values (σ_1, ϵ), the values of λ were calculated for 10 realisations of the white noise. The open circles plotted in Figure 8 are the means of λ from these ensembles, while the errorbars denote the ± 1 standard deviation range. The variation of λ with σ_1 is similar for each of the values of ϵ considered. The leading Lyapunov exponents of the deterministic system ($\sigma_1 = 0$) are negative. As σ_1 increases from zero, λ initially decreases: the presence of very weak noise has a stabilising influence upon the system. As σ_1 is increased further, λ eventually begins to increase, and for sufficiently large weather fluctuations changes sign. The noise level at which the leading Lyapunov exponent switches from negative to positive decreases for decreasing ϵ. Figure 9 displays λ as a function of σ_1 for $\log_{10}\epsilon = -2.3$, over the region in which it changes sign. For this value of the mechanical damping, even very weak fluctuations in the mechanical forcing can change the sign of the leading Lyapunov exponent, and induce sensitivity of the climate system to initial conditions.

We now consider the effects of fluctuations in buoyancy forcing on λ. Figure 10 displays the dependence of λ on σ_2 for $\sigma_1 = 0$ and $\log_{10}\epsilon = -2.1, -2.2$. As was the case with varying σ_1, λ first decreases with σ_2 from the deterministic value, reaches a minimum value, then begins to increase, eventually becoming positive. Figure 11 displays λ as a function of σ_2 for $\sigma_1 = 0$ and $\log_{10}\epsilon = -2.3$. As was the case with fluctuations in the mechanical forcing, even weak weather variability in the buoyancy forcing can render the leading Lyapunov exponent positive for $\log_{10}\epsilon = -2.3$.

For the parameter values considered, it appears that, generically, the effect of fluctuations in both buoyancy forcing and mechanical forcing on the leading Lyapunov exponent of the

thermally-direct branch of the Maas model is first to decrease λ relative to the deterministic value, and then to increase λ as the fluctuations become stronger. Eventually, the presence of fluctuations changes the sign of λ from negative to positive, and the climate state is rendered sensitive to initial conditions.

As discussed in Section 1, the presence of stochastic fluctuations in the system will have an impact on predictability irrespective of the sign of the leading Lyapunov exponent. By definition, the weather noise is unpredictable. If the fluctuations are sufficiently strong that the stochastic trajectories deviate substantially from the deterministic ones, then these fluctuations themselves will limit predictability. If, however, individual realisations of $\nabla\overline{\rho}(t)$ evolve close to the deterministic attractor, then the sign of the Lyapunov exponents may play a key role in determining predictability. To demonstrate this, the following experiment was carried out.

Figures 8 and 9 show that λ is negative for $\log_{10}\epsilon = -2.2$ and positive for $\log_{10}\epsilon = -2.3$ for noise levels $\sigma_1 = .07, \sigma_2 = 0$. One hundred realisations of $\nabla\overline{\rho}(t)$ with random, but nearby, initial conditions and different realisations of the weather noise process $\dot{W}_1$ were computed at this noise level for both of these friction values. Each one of these realisations can be considered the "true" trajectory of the climate state, and each of the 99 remaining a "prediction". For each of the 4950 resulting pairs of "true" and "forecast" trajectories, a time series of correlation coefficients within a sliding window of width $\Delta t = 0.5$ between the "true" and "forecast" $\overline{\rho}_x(t)$ time series was generated. This window is wide enough to resolve several complete circuits of the limit cycle. The resulting time series of correlations characterises the evolution of local phase differences between the "true" and "forecast" trajectories. Figures 12(a) and (c) display the evolution in time of the estimated probability density function (PDF) of the windowed correlation coefficient for $\log_{10}\epsilon = -2.2$ and $\log_{10}\epsilon = -2.3$, respectively. For both values of ϵ, the distribution is initially concentrated near 1: the different trajectories are all initially very similar. As time increases, both PDFs broaden, indicating increasingly likely dephasing between "true" and "forecast" trajectories. For $\log_{10}\epsilon = -2.2$, most of the mass of the PDF remains near 1 as t increases; this implies that despite the stochastic fluctuations, there is usually only limited dephasing between trajectories and the

climate state retains a substantial degree of predictability. However, for $\log_{10}\epsilon = -2.3$, the PDF rapidly broadens and flattens out, indicating a general rapid dephasing and loss of predictability. The thick line in Figures 12(a) and (c) corresponds to the average windowed correlation coefficient; this clearly decreases much more rapidly for $\log_{10}\epsilon = -2.3$ than for $\log_{10}\epsilon = -2.2$. The difference in evolution of the windowed correlation coefficient is a consequence of the fact that for $\log_{10}\epsilon = -2.3$, the leading Lyapunov exponent is positive, while for $\log_{10}\epsilon = -2.2$, it is negative. Clearly, in the presence of weather fluctuations sufficiently weak that the trajectories of the climate variable do not differ too much from the deterministic attractor, the sign of the leading Lyapunov exponent has a substantial impact on the predictability of the system.

The above analysis investigated the rate of decorrelation rate between individual realisations of the climate trajectory. Figures 12(b) and (d) display the distribution of the windowed correlation coefficient between each individual realisation and the ensemble average of the remaining 99. For both $\log_{10}\epsilon = -2.2$ and $\log_{10}\epsilon = -2.3$, the decorrelation rate is smaller for the ensemble forecasts than it is for individual forecasts. Again, the windowed correlation coefficient distribution for $\log_{10}\epsilon = -2.3$ broadens and flattens much more rapidly than for $\log_{10}\epsilon = -2.2$, demonstrating the limits on predictability induced by positive λ.

This experiment was repeated with $\sigma_1 = 0.75, \sigma_2 = 0$ for the friction parameter values $\log_{10}\epsilon = -2.2$ and $\log_{10}\epsilon = -2.1$. The results (not shown) demonstrate that the different trajectories decorrelate at about the same rate for both values of ϵ. At this noise level, the effects of the weather fluctuations on the predictability of the climate system dominate over those associated with the sign of λ.

6 Conclusions

In this study, we have considered the dynamics of a low-order, nonlinear model of the thermally and wind-driven ocean circulation proposed by Maas (1994). This model is attractive in that it can be obtained rigorously from the primitive equations via a clear sequence of approximations, although it is clearly too simple to provide an accurate quantitative repre-

sentation of ocean dynamics.. The Maas model displays multiple regimes of circulation and a rich variety of behaviour over realistic parameter ranges, including limit cycles and deterministic chaos. The original formulation of the Maas model considered the evolution of the ocean state (the climate) in the absence of fluctuations associated with weather variability; the mechanical and buoyancy forcings were represented as fixed parameters. In the present study, variability on scales not represented explicitly (weather fluctuations) has been parameterised as stochastic fluctuations in these forcing parameters. The primary question we have addressed is the issue of how these fluctuations affect the predictability of the system, as measured by the leading Lyapunov exponent. It was demonstrated numerically that the presence of even very weak weather fluctuations can change the sign of the leading Lyapunov exponent of the climate state from negative to positive. The climate system is then sensitive to initial conditions, and is characterised by a finite predictability time. Of course, the presence of (by definition) unpredictable stochastic fluctuations also limits the predictability of the system. We have demonstrated that if the fluctuations are sufficiently small that individual stochastic trajectories do not deviate too far from the deterministic attractor, then the sign of the leading Lyapunov exponent has a determining impact on predictability.

The present study suggests a number of natural extensions. First, as was discussed in Section 2, it has been assumed that the statistics of the weather variables are independent of the climate state, i.e., the weather drives the climate state but not vice versa. A natural extension of this study would be an investigation of the extent to which two-way coupling between the climate and weather variables would change the dynamical behaviour of the model. Second, the effect of including weather variability on the more general model introduced by van der Schrier and Maas (1998), in which the density field is determined by both salinity and temperature, could be considered. A third natural extension is to relax the assumptions (13)-(16). In particular, the effect on the dynamics of having these assumptions hold in the time mean, but not instantaneously, could be considered. Finally, a detailed consideration of the effects of high-frequency variability on the Lyapunov exponents of more complex (and more climatically relevant) models would be an important extension of this study.

The problem of predictability is subtle (Palmer, 1995): the leading Lyapunov exponent is a bulk quantity characterising the average growth rate of perturbations over the entire trajectory of the climate state. Analysis of the predictability of flows starting from a particular climate state involves consideration of the associated singular value spectrum (Palmer, 1995; Farrell and Ioannou, 1996a). In many cases, this local measure of error growth may be more relevant than the global measure associated with λ. Furthermore, the leading Lyapunov exponent may not be directly related to predictability time in spatially extended systems characterised by spatio-temporal chaos (e.g. Paladin and Vulpiani, 1994; Boffetta et al., 2002). In such systems, the predictability time may be more directly related to the time needed for an initial perturbation to propagate through the system or to align itself along the direction of most rapid error growth, or large-scale structure in the system may be predictable despite the presentce of unpredictable microscopic fluctuations. Whether or not the leading Lyapunov exponent is a primary determinant of predictability for general hydrodynamical systems is unclear, although it appears to be so in the shell model of three-dimensional turbulence described in Paladin and Vulpiani (1994). Finally, even if the leading Lyapunov exponent is an important measure of the predictability of oceanic circulation, the noise effects detailed above in the context of Maas' reduced model may not appear in the original set of partial differential equations; this question can only be addressed through the study of less idealised models. The goal of the present study is not to claim that fluctuations will necessarily render the ocean circulation unpredictable; rather, it is to suggest that fluctuations may alter the sign of the leading Lyapunov exponent, which may have consequences for the predictability of the climate system.

A general feature of current generation General Circulation Models (GCMs) is that they underestimate the observed variability of the climate system (e.g. Barsugli and Battisti, 1998). To a certain extent, this is because these models are all characterised by finite temporal and spatial resolution. Variability below these scales is generally represented as a deterministic function of the resolved variables, or ignored. Because most of this subgrid-scale variability is associated with turbulent motion, it has an inherently random character. It is conceivable that rather than the deterministic representation in terms of the resolved

variables, subgrid scale processes - that is, the weather variables - are more appropriately modelled stochastically. Stochastic subgrid-scale parameterisation in GCMs has been advocated by Palmer (2001); some preliminary results in this direction have recently been presented by Lin and Neelin (2000). In the context of the very simple model considered in this study, it has been shown that the neglect of weak stochastic fluctuations can affect the sign of the leading Lyapunov exponents, with potentially pronounced implications for the predictability of the system. It is possible that the stochastic representation of subgrid-scale variability even in complex GCMs may have a substantial impact on their ability to represent the observed climate system.

Acknowledgements

The author is grateful to Peter Imkeller for suggestions and helpful comments. The manuscript was considerably improved by the comments of two anonymous referees. This work was supported by DFG Schwerpunktprogramm "Interagierende stochastische Systeme von hoher Komplexität".

Appendix A: Lyapunov Exponents of Stochastic Differential Equations

A basic account of Lyapunov exponents for SDEs is presented in Kloeden and Platen (1992). An overview of the results is presented in this appendix.

We consider the Stratonovich SDE in $\Re^d$

$$d\mathbf{X}(t) = \mathbf{a}(\mathbf{X}(t))dt + b(\mathbf{X}(t)) \circ d\mathbf{W}(t), \tag{67}$$

in which $\mathbf{W}(t)$ is a p-dimensional Wiener process with independent components. This equation may be written

$$d\mathbf{X}(t) = \mathbf{a}(\mathbf{X}(t))dt + \sum_{k=1}^{p} \mathbf{b}^k(\mathbf{X}(t)) \circ dW_k(t). \tag{68}$$

A discussion of the difference between Ito and Stratonovich SDEs, and the rules for transformation between the two, is presented in Gardiner (1997). As in deterministic systems, Lyapunov exponents characterise the stability of small perturbations, $\mathbf{Z}(t) = \mathbf{X}(t) - \hat{\mathbf{X}}(t)$, around a realisation $\hat{\mathbf{X}}(t)$ of (68). The process $\mathbf{Z}(t)$ is described by the linearisation of (68) around $\hat{\mathbf{X}}(t)$:

$$d\mathbf{Z}(t) = A(\hat{\mathbf{X}}(t))\mathbf{Z}(t)dt + \sum_{k=1}^{p} B^k(\hat{\mathbf{X}}(t))\mathbf{Z}(t) \circ dW_k(t) \quad ; \quad \mathbf{Z}(0) = \mathbf{Z}_0, \tag{69}$$

where the matrices A and B^k are given by

$$A(\hat{\mathbf{X}}(t))_{ij} = \partial_{x_j} a_i(\hat{\mathbf{X}}(t)) \tag{70}$$

$$B^k(\hat{\mathbf{X}}(t))_{ij} = \partial_{x_j} b_i^k(\hat{\mathbf{X}}(t)). \tag{71}$$

A Lyapunov exponent of the system (68) is defined as the limit:

$$\lambda(z_0) = \lim_{t\to\infty} \frac{\ln ||\mathbf{Z}(t)||}{t}, \tag{72}$$

where $||\cdot||$ denotes the L^2 norm. The Multiplicative Ergodic Theorem of Oseledec (Arnold, 1998) guarantees that for general z_0 (that is, excluding a set of measure zero), the limit (72) will be unique and correspond to the largest Lyapunov exponent of the system (68), denoted λ.

As the definition of the Lyapunov exponent involves only the norm of the process $\mathbf{Z}(t)$, it is convenient to consider (69) in spherical coordinates. Define

$$R(t) = ||\mathbf{Z}(t)|| \tag{73}$$

$$\mathbf{S}(t) = \frac{\mathbf{Z}(t)}{||\mathbf{Z}(t)||}, \tag{74}$$

so that $\mathbf{S}(t)$ is a process on the unit sphere in $\Re^d$. Because equation (69) is a Stratonovich SDE, the regular rules of calculus apply, so $R(t)$ and $\mathbf{S}(t)$ satisfy the SDEs:

$$dR = q^0(\mathbf{S})Rdt + \sum_{k=1}^{p} q^k(\mathbf{S})R \circ dW_k \tag{75}$$

$$d\mathbf{S} = (A(\hat{\mathbf{X}}) - q^0(\mathbf{S})I)\mathbf{S}dt + \sum_{k=1}^{p}(B^k(\hat{\mathbf{X}}) - q^k(\mathbf{S})I)\mathbf{S} \circ dW_k, \tag{76}$$

where

$$q^0(\mathbf{S}(t)) = \mathbf{S}(t)^T A \mathbf{S}(t), \tag{77}$$

$$q^k(\mathbf{S}(t)) = \mathbf{S}(t)^T B^k \mathbf{S}(t), \tag{78}$$

and I denotes the identity matrix in $\Re^d$. Equation (75) may be formally integrated to yield

$$\ln R(t) = \int_0^t q^0(\mathbf{S}(u))du + \sum_{k=1}^{p} \int_0^t q^k(\mathbf{S}(u)) \circ dW_k(u) \tag{79}$$

$$= \int_0^t q(\mathbf{S}(u))du + \sum_{k=1}^{p} \int_0^t q^k(\mathbf{S}(u))dW_k(u), \tag{80}$$

where in the last equality we have transformed the Stratonovich integral into an Ito integral, so that

$$q(\mathbf{S}) = q^0(\mathbf{S}) + \sum_{k=1}^{p} \left(\frac{1}{2} \mathbf{S}^T [B^k(\hat{\mathbf{X}}) + B^k(\hat{\mathbf{X}})^T] B^k(\hat{\mathbf{X}}) \mathbf{S} - (q^k(\mathbf{S}))^2 \right). \tag{81}$$

The transformation to an Ito integral is carried out to take advantage of the fact that, with probability one,

$$\lim_{t \to \infty} \frac{1}{t} \int_0^t Y(s) dW(s) = 0 \tag{82}$$

for any (relevant) stochastic process Y_s. Consequently, we find the following equation for the leading Lyapunov exponent of (68):

$$\lambda = \lim_{t \to \infty} \frac{1}{t} \ln ||\mathbf{Z}(t)|| \tag{83}$$

$$= \lim_{t \to \infty} \frac{1}{t} \ln R(t) \tag{84}$$

$$= \lim_{t \to \infty} \frac{1}{t} \int_0^t q(\mathbf{S}_u) du. \tag{85}$$

Note that equation (76) is an SDE for $\mathbf{S}(t)$ alone; it does not depend on the process $R(t)$. Thus, the leading Lyapunov exponent of the SDE (68) may be evaluated by solving the SDE (76) and evaluating (85).

References

Arnold, L (1998). Random dynamical systems. Springer, Berlin, 586 pp

Arnold L, Imkeller P, Sri Namachchivaya N (2001) The asymptotic stability of a noisy nonlinear oscillator. Submitted.

Barsugli JJ, Battisti DS (1998) The basic effects of atmosphere-ocean thermal coupling on midlatitude variability. J Atmos Sci 55: 477-493

Balusara A, Jacobs E, Schieve, W (1990) Noise effects in a nonlinear dynamic system: The rf superconducting quantum interference device. Phys Rev A42: 4614-4621

Boffetta G, Cencini M, Falcioni M, Vulpiani A (2002) Predictability: a way to characterize complexity. Phys Rep 356: 367-474

Delworth TL, Greatbatch RJ (2000) Multidecadal thermohaline circulation variability driven by atmospheric surface flux forcing. J Climate 13: 1481-1495

Farrell BF, Ioannou PJ (1996b) Generalized stability theory. Part II: Nonautonomous operators. J Atmos Sci 53: 2041-2053

Farrell BF, Ioannou PJ (1999) Perturbation growth and structure in time-dependent flows. J Atmos Sci 56: 3622-3639

Gardiner CW (1997) Handbook of stochastic methods for physics, chemistry, and the natural sciences. Springer, Berlin, 442 pp

Griffies SM, Tziperman E (1995) A linear thermohaline oscillator driven by stochastic atmospheric forcing. J Climate 8: 2440-2453

Hasselmann K (1976) Stochastic climate models. Tellus 28:473-484

Kloeden PE, Platen E (1992) Numerical solution of stochastic differential equations. Springer, Berlin, 632 pp

Lin JW-B, Neelin JD (2000) Influence of a stochastic moist convective parameterisation on tropical climate variability. Geophys Res Lett 27: 3691-3694

Maas LRM (1994) A simple model for the three-dimensional, thermally and wind-driven ocean circulation. Tellus 46A: 671-680

Monahan AH (2001) Stabilisation of climate regimes by noise in a simple model of the

thermohaline circulation. J Phys Oceanogr, submitted.

Monahan AH, Timmermann A, Lohmann G (2001) Comments on "Noise-induced transitions in a simplified model of the thermohaline circulation". J Phys Oceanogr, in press

Moore AM (1999) Wind-induced variability of ocean gyres. Dyn Atmos Ocean 29:335-364

Ott E (1993) Chaos in dynamical systems. Cambridge University Press, Cambridge, 385 pp

Paladin G, Vulpiani A (1994) Predictability in spatially extended systems. J Phys A 27: 4911-4917.

Palmer TN (1995) Predictability of the atmosphere and oceans: From days to decades. Predictability, ECMWF Seminar Proceedings, 4-8 September 1995

Palmer TN (2001) A nonlinear dynamical perspective on model error: A proposal for nonlocal stochastic-dynamic parameterisation in weather and climate prediction models. QJ Roy Meteo Soc 127: 279-304

Penland C (2001) A stochastic approach to nonlinear dynamics: A review. Bull Am Met Soc, submitted

Penland C, Flügel M, Chang P (2000) Identification of dynamical regimes in an intermediate coupled ocean-atmospheric model. J Climate 13: 2105-2115

Schimansky-Geier L, Herzel H (1993) Positive Lyapunov exponents in the Kramers oscillator. J Stat Phys 70: 141-147

Timmermann A, Latif M, Voss R, Grotzner A (1998) Northern Hemispheric interdecadal variability: A coupled air-sea mode. J Climate 11: 1906-1931

van der Schrier G (2000) Aspects of the thermohaline circulation in a simple model. PhD Thesis, KNMI, The Netherlands.

van der Schrier G, Maas LRM (1998) Chaos in a simple model of the three-dimensional, salt-dominated ocean circulation. Clim Dynamics 14: 489-502

Figure Captions

Figure 1:Stationary solutions $(\overline{\rho}_x^*, \overline{\rho}_y^*, \overline{\rho}_z^*)$ of equations (33)-(35) as functions of ϵ. Solid (dashed) lines denote stable (unstable) fixed points.

Figure 2: As in Figure 1, but for the fixed points of the x- and $y-$ components of the angular momentum.

Figure 3: Leading Lyapunov exponent λ (upper panel) and values of $\overline{\rho}_x$ at which the trajectory crosses the surface $\overline{\rho}_y = \overline{\rho}_y^*$ (lower panel) as a function of ϵ, on the thermally-direct branch.

Figure 4: Deterministic attractors of thermally-direct branch for $\log_{10}\epsilon = (a) - 1.8, (b) - 2.2, (c) - 2.3, (d) - 2.4$.

Figure 5: A blow-up of Figure 3.

Figure 6: As in Figure 4, with $\sigma_1 = 0.1, \sigma_2 = 0$.

Figure 7: As in Figure 4, with $\sigma_1 = 1, \sigma_2 = 0$.

Figure 8: Leading Lyapunov exponents of the stochastic Maas model as a function of σ_1 for $\sigma_2 = 0$, $\log_{10}\epsilon = -2.0$ (thin line), -2.1 (dash-dotted line), and -2.2 (thick line).

Figure 9: As in Figure 8 for $\sigma_2 = 0$, $\log_{10}\epsilon = -2.3$.

Figure 10: Plot of λ as a function of σ_2 for $\sigma_1 = 0$ and $\log_{10}\epsilon = -2.1$ (thin line) and $\log_{10}\epsilon = -2.2$ (thick line).

Figure 11: As in Figure 10 for $\sigma_1 = 0$, $\log_{10}\epsilon = -2.3$.

Figure 12: Time evolution of the PDFs of the windowed correlation coefficient between (a) "true" and individual "forecast" $\overline{\rho}_x$ trajectories and (b) "true" and ensemble mean "forecast" trajectories for $\log_{10}\epsilon = -2.2$. (c) and (d) are as (a) and (b) for $\log_{10}\epsilon = -2.3$. The thick lines are the ensemble means of the windowed correlation coefficients.

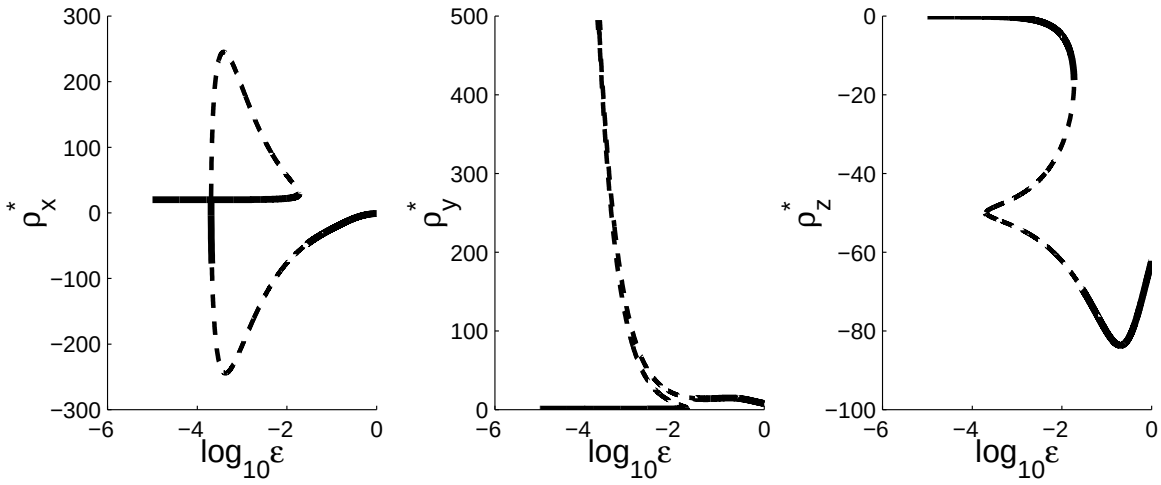

Figure 1: Stationary solutions $(\overline{\rho}_x^*, \overline{\rho}_y^*, \overline{\rho}_z^*)$ of equations (33)-(35) as functions of ϵ. Solid (dashed) lines denote stable (unstable) fixed points.

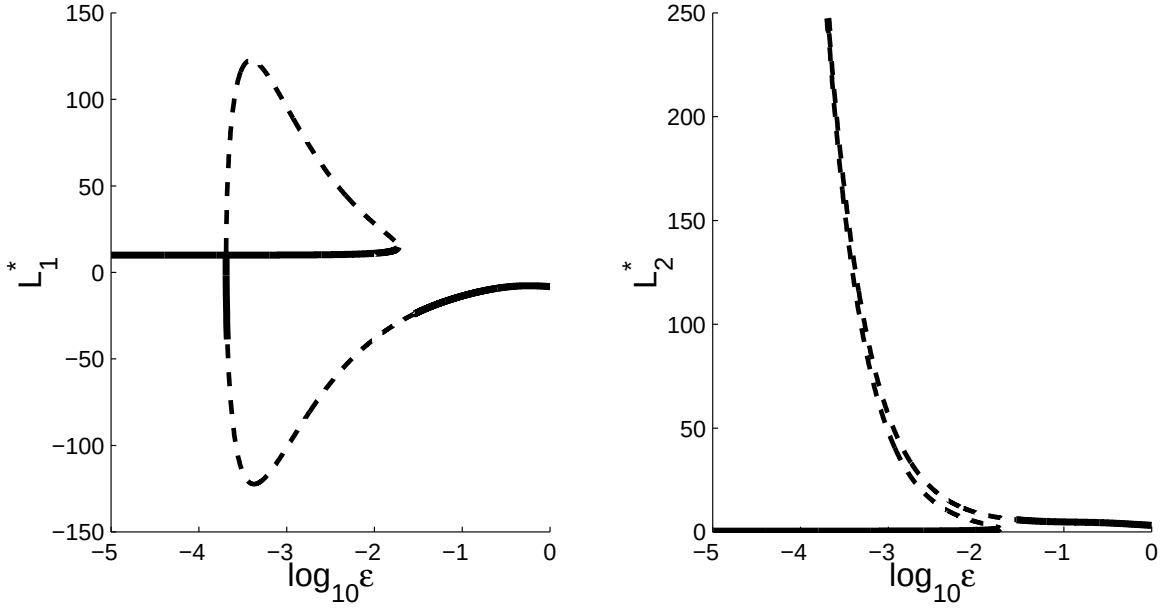

Figure 2: As in Figure 1, but for the fixed points of the x- and $y-$ components of the angular momentum.

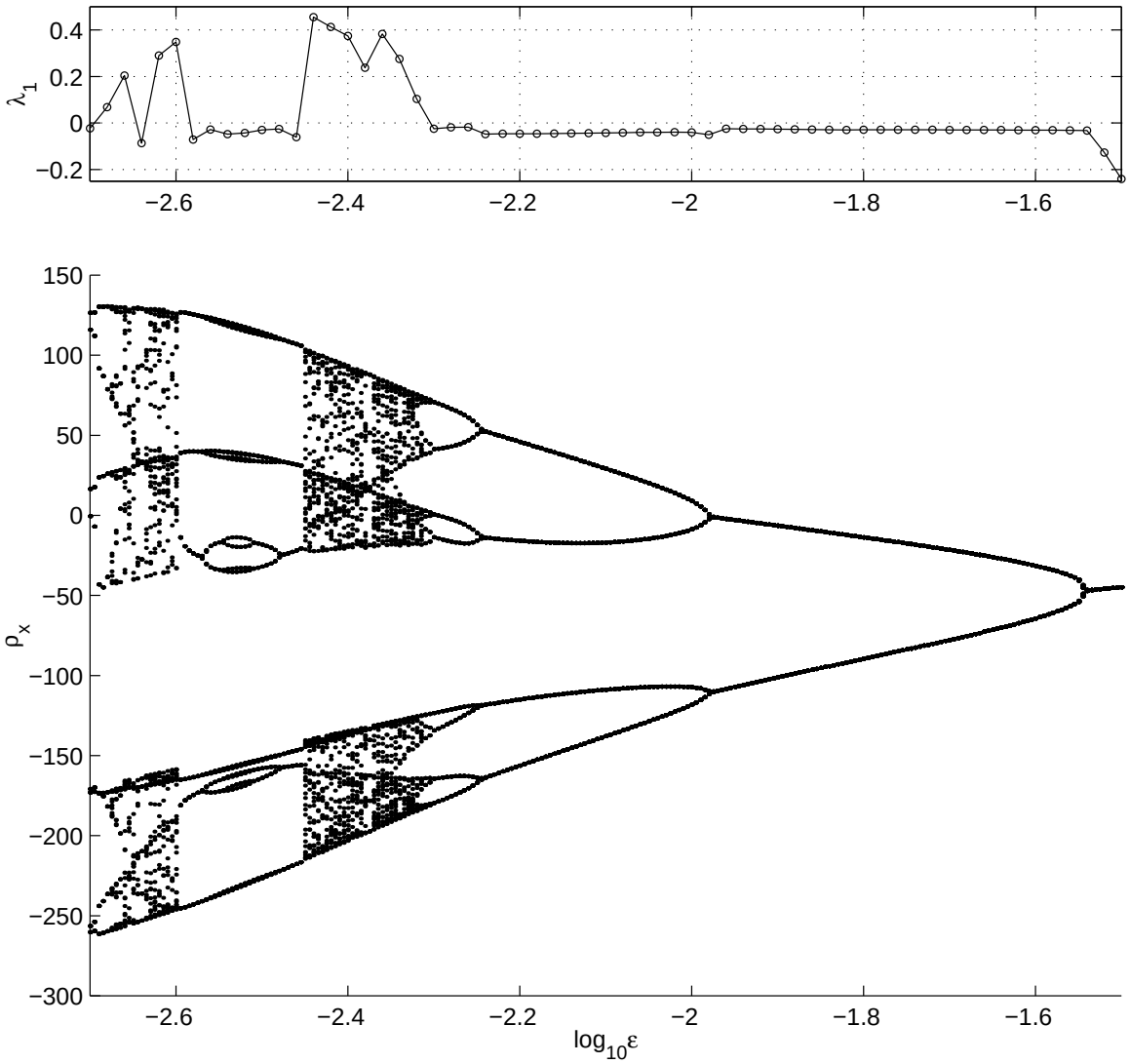

Figure 3: Leading Lyapunov exponent λ (upper panel) and values of $\overline{\rho}_x$ at which the trajectory crosses the surface $\overline{\rho}_y = \overline{\rho}_y^*$ (lower panel) as a function of ϵ, on the thermally-direct branch.

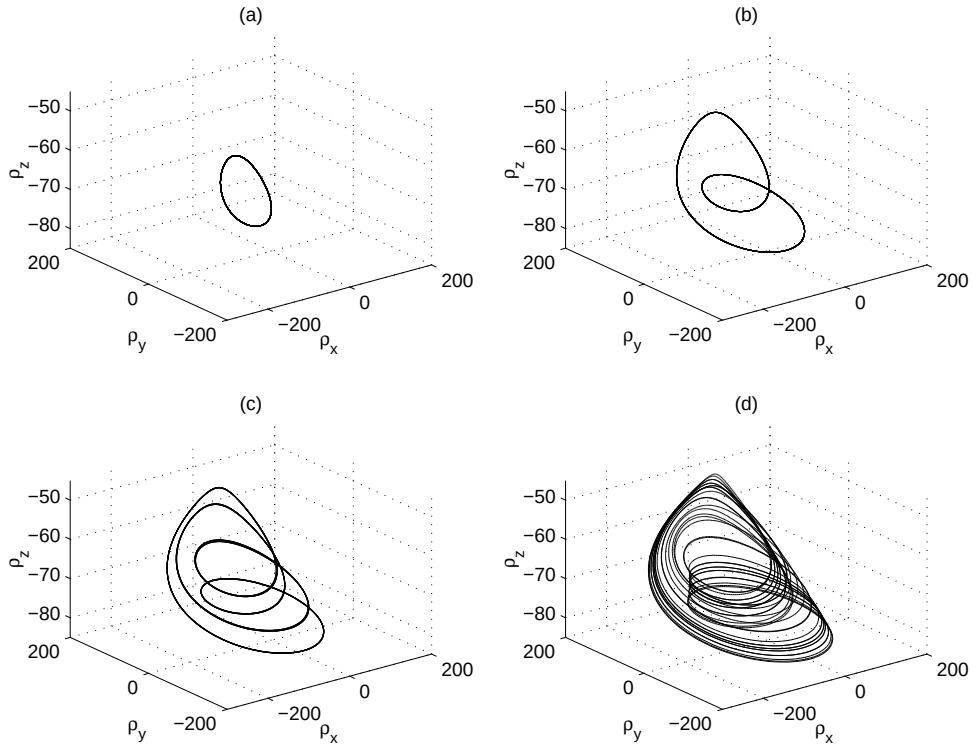

Figure 4: Deterministic attractors of thermally-direct branch for $\log_{10}\epsilon = (a) - 1.8, (b) - 2.2, (c) - 2.3, (d) - 2.4$.

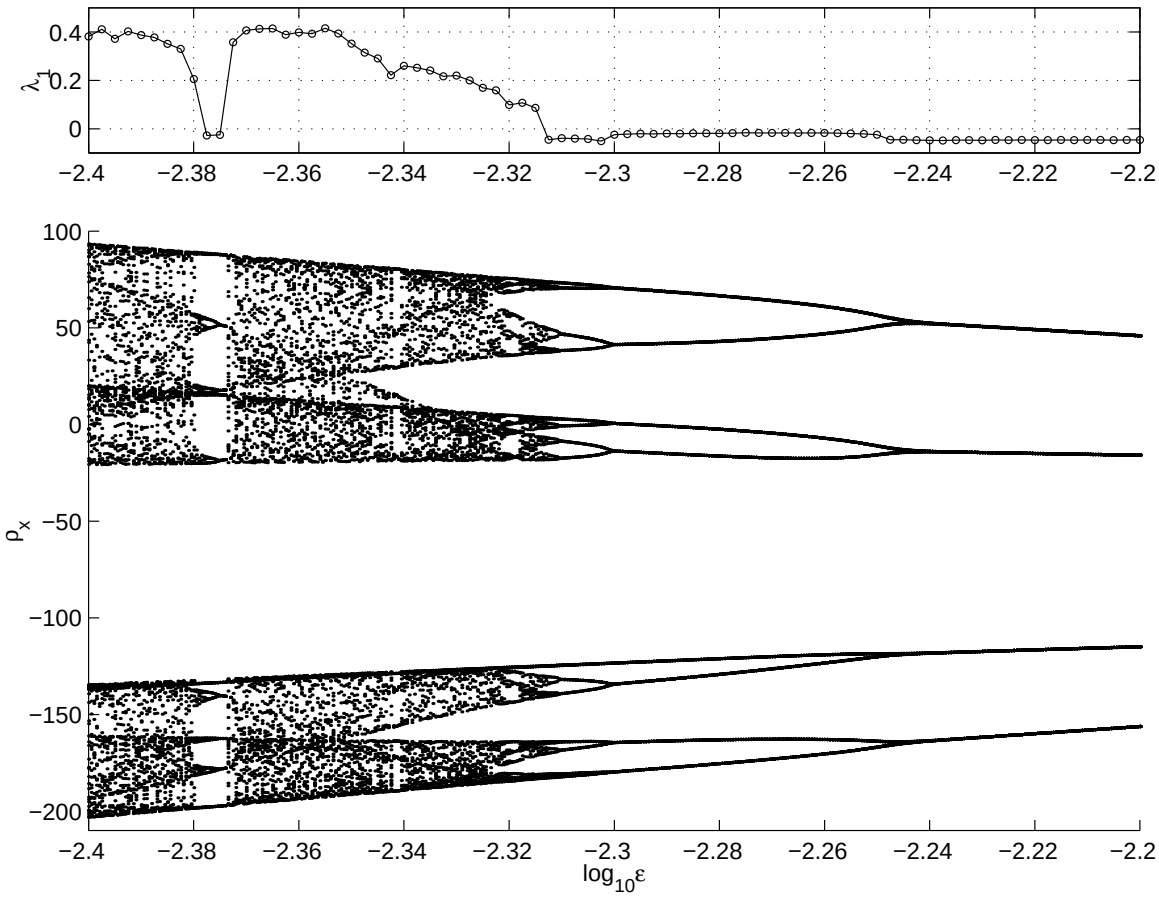

Figure 5: A blow-up of Figure 3.

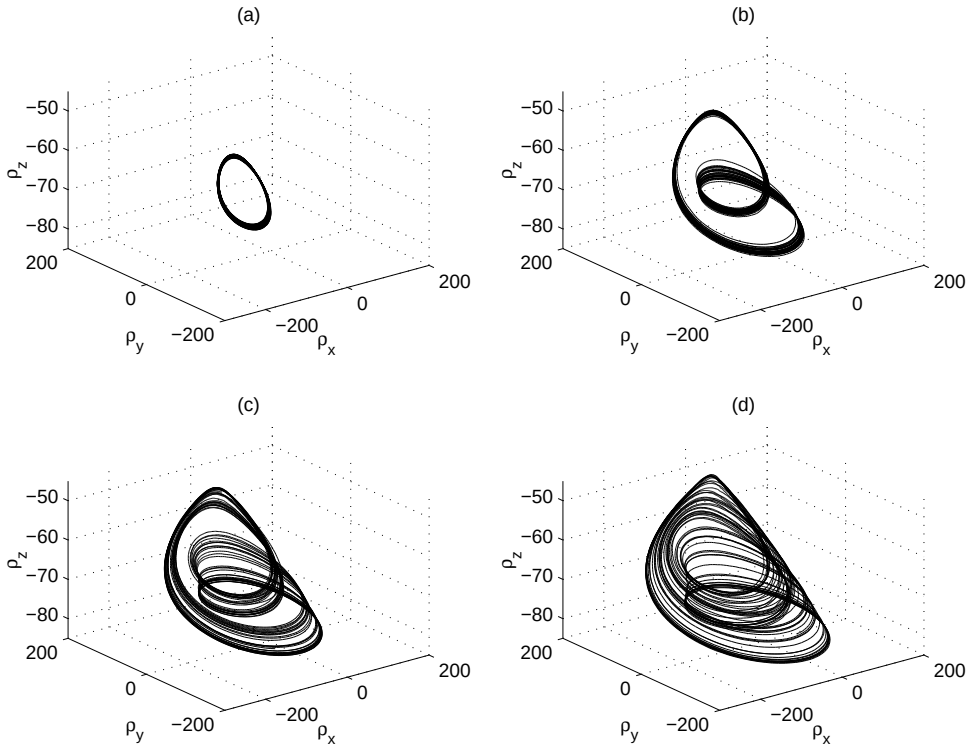

Figure 6: As in Figure 4, with $\sigma_1 = 0.1, \sigma_2 = 0$.

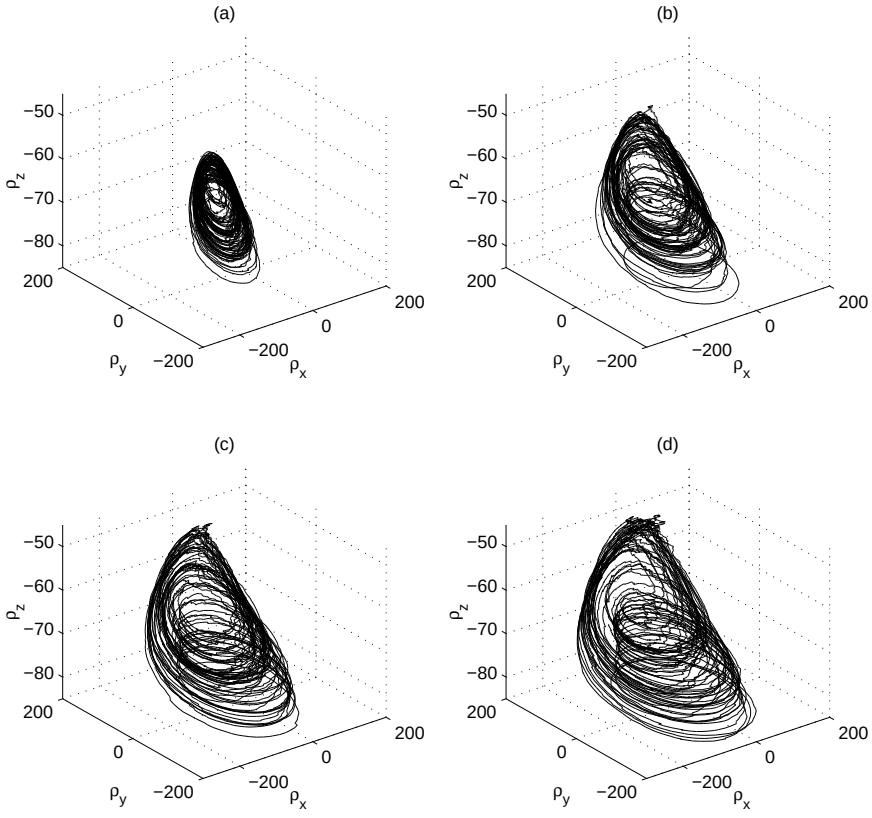

Figure 7: As in Figure 4, with $\sigma_1 = 1, \sigma_2 = 0$.

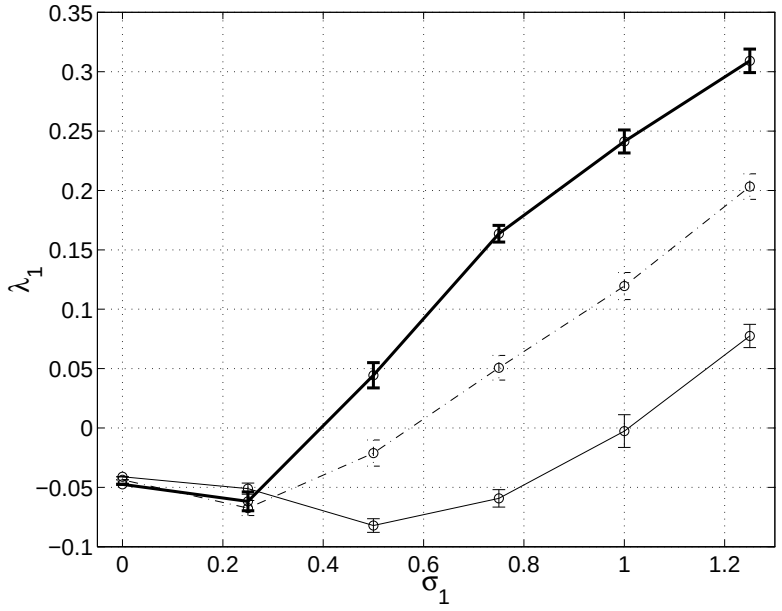

Figure 8: Leading Lyapunov exponents of the stochastic Maas model as a function of σ_1 for $\sigma_2 = 0$, $\log_{10}\epsilon = -2.0$ (thin line), -2.1 (dash-dotted line), and -2.2 (thick line).

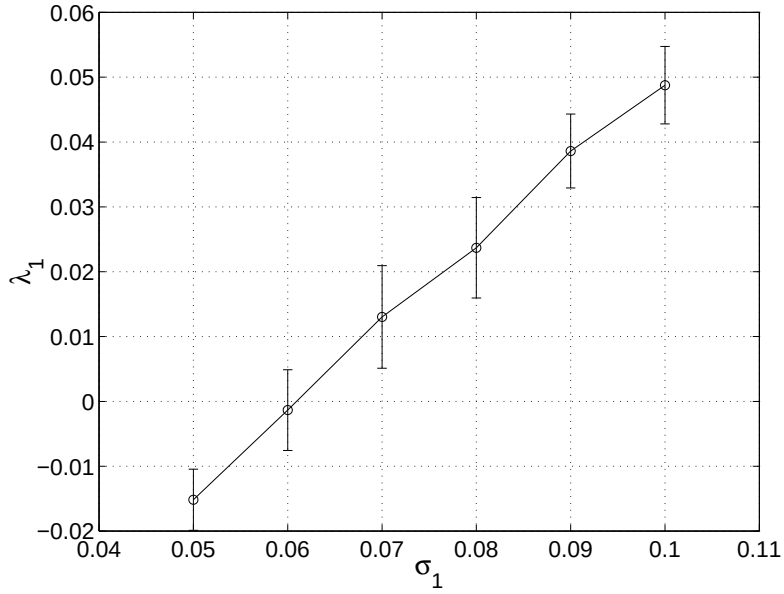

Figure 9: As in Figure 8 for $\sigma_2 = 0$, $\log_{10}\epsilon = -2.3$.

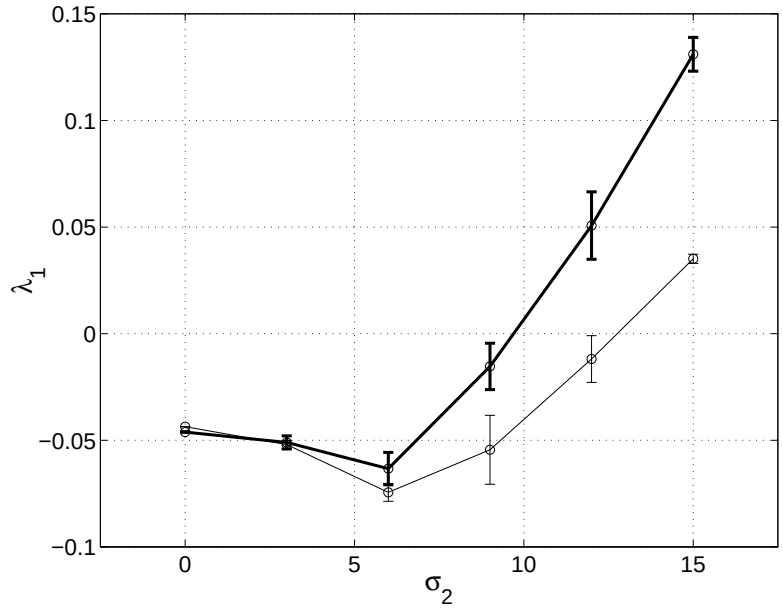

Figure 10: Plot of λ as a function of σ_2 for $\sigma_1 = 0$ and $\log_{10}\epsilon = -2.1$ (thin line) and $\log_{10}\epsilon = -2.2$ (thick line).

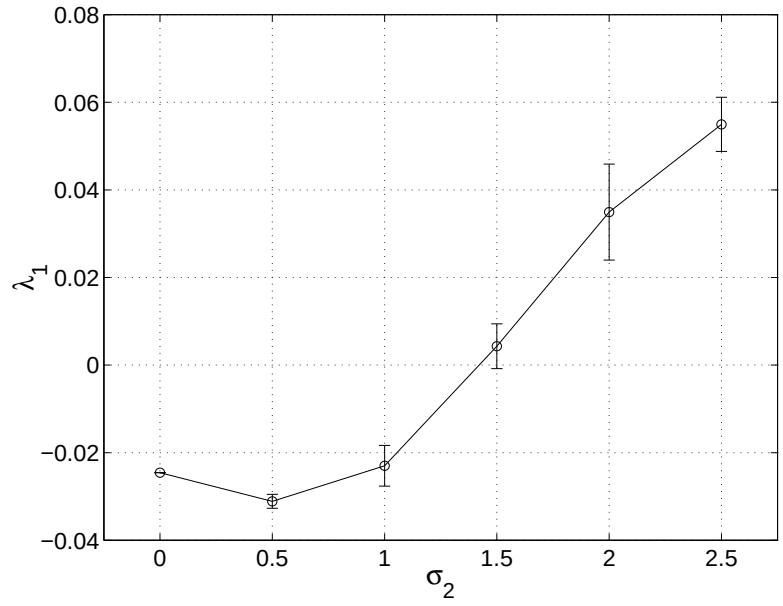

Figure 11: As in Figure 10 for $\sigma_1 = 0$, $\log_{10}\epsilon = -2.3$.

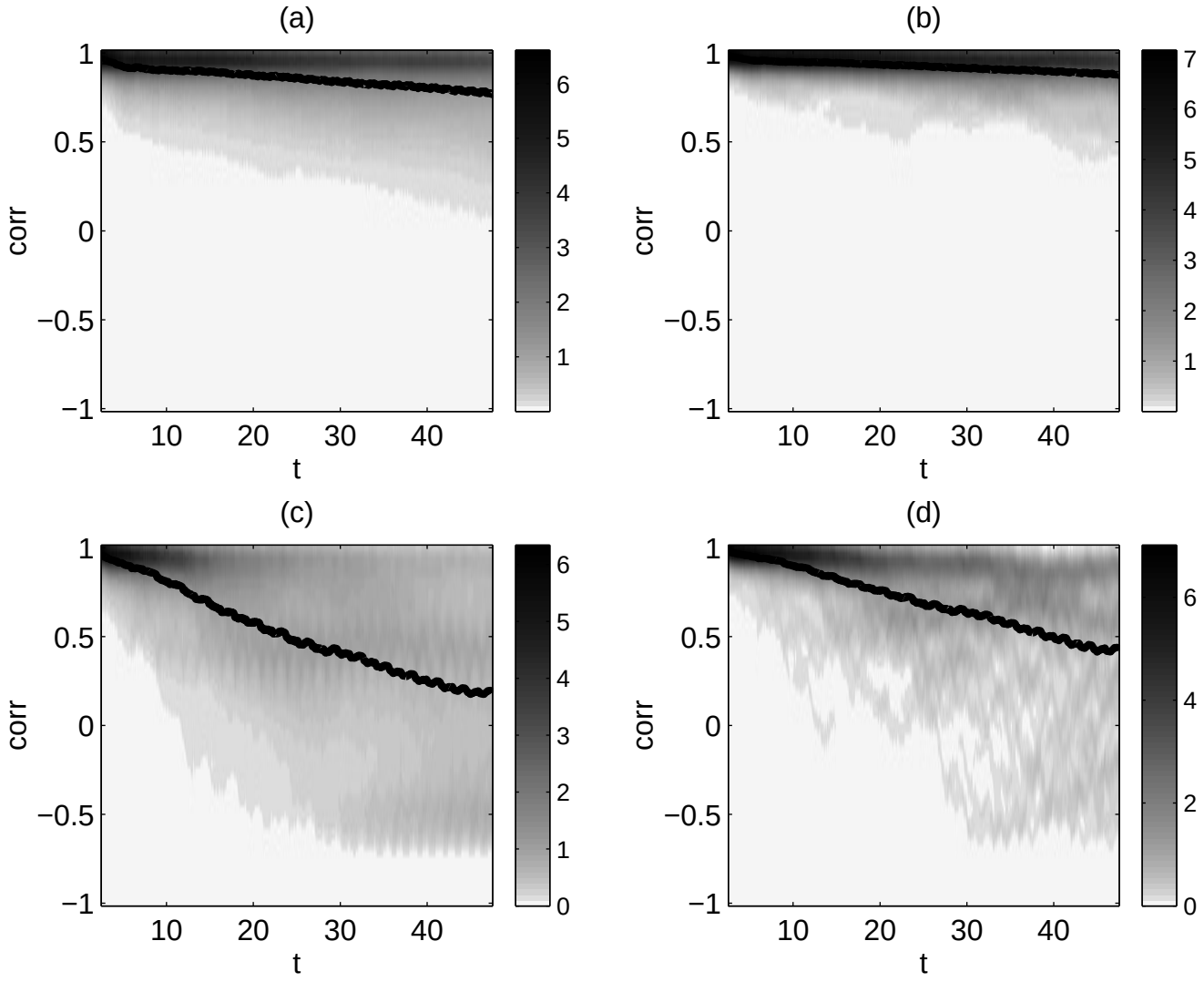

Figure 12: Time evolution of the PDFs of the windowed correlation coefficient between (a) "true" and individual "forecast" $\overline{\rho}_x$ trajectories and (b) "true" and ensemble mean "forecast" trajectories for $\log_{10}\epsilon = -2.2$. (c) and (d) are as (a) and (b) for $\log_{10}\epsilon = -2.3$. The thick lines are the ensemble means of the windowed correlation coefficients.